# First-in-Humans PET Imaging of Tissue Factor in Patients with Primary and Metastatic Cancers Using $^{18}$F-labeled Active-Site Inhibited Factor VII ($^{18}$F-ASIS): Potential as Companion Diagnostic

Mathias Loft*[1], Camilla Christensen*[1], Malene M. Clausen[1,2], Esben A. Carlsen[1], Carsten P. Hansen[3], Niels Kroman[4], Seppo W. Langer[2,5], Claus Høgdall[6], Jacob Madsen[1], Nic Gillings[1], Carsten H. Nielsen[1,7], Thomas L. Klausen[1], Søren Holm[1], Annika Loft[1], Anne K. Berthelsen[1], and Andreas Kjaer[1]

[1]*Department of Clinical Physiology and Nuclear Medicine & Cluster for Molecular Imaging, Copenhagen University Hospital – Rigshospitalet & Department of Biomedical Sciences, University of Copenhagen, Denmark;* [2]*Department of Oncology, Copenhagen University Hospital – Rigshospitalet, Denmark;* [3]*Department of Surgery, Copenhagen University Hospital – Rigshospitalet, Denmark;* [4]*Department of Breast Surgery, Copenhagen University Hospital – Rigshospitalet, Denmark;* [5]*Department of Clinical Medicine, University of Copenhagen, Denmark;* [6]*Department of Gynecology, Copenhagen University Hospital – Rigshospitalet, Denmark and* [7]*Minerva Imaging ApS, Denmark*

Tissue factor (TF) expression in cancers correlates with poor prognosis. Recently, the first TF-targeted therapy was approved by the U.S. Food and Drug Administration for cervical cancer. To unfold the potential of TF-targeted therapies, correct stratification and selection of patients eligible for treatments may become important for optimization of patient outcomes. TF-targeted PET imaging based on $^{18}$F-radiolabeled active-site inhibited versions of the TF natural ligand coagulation factor VII ($^{18}$F-ASIS) has in preclinical models convincingly demonstrated its use for noninvasive quantitative measurements of TF expression in tumor tissue. $^{18}$F-ASIS PET imaging thus has the potential to act as a diagnostic companion for TF-targeted therapies in the clinical setting. **Methods:** In this first-in-humans trial, we included 10 cancer patients (4 pancreatic, 3 breast, 2 lung, and 1 cervical cancer) for $^{18}$F-ASIS PET imaging. The mean and SD of administered $^{18}$F-ASIS activity was 157 ± 35 MBq (range, 93–198 MBq). PET/CT was performed after 1, 2, and 4 h. The primary objectives were to establish the safety, biodistribution, pharmacokinetics, and dosimetry of $^{18}$F-ASIS. Secondary objectives included quantitative measurements of SUVs in tumor tissue with PET and evaluation of the correlation (Pearson correlation) between tumor $SUV_{max}$ and ex vivo TF expression in tumor tissue. **Results:** Administration of $^{18}$F-ASIS was safe, and no adverse events were observed. No clinically significant changes in vital signs, electrocardiograms, or blood parameters were observed after injection of $^{18}$F-ASIS. Mean $^{18}$F-ASIS plasma half-life was 3.2 ± 0.6 h, and the radiotracer was predominantly excreted in the urine. For injection activity of 200 MBq of $^{18}$F-ASIS, effective whole-body dose was 4 mSv and no prohibitive organ-specific absorbed doses were found. Heterogeneous radiotracer uptake was observed across patients and within tumors. We found a trend of a positive correlation between tumor $SUV_{max}$ and ex vivo TF expression ($r = 0.84$, $P = 0.08$, $n = 5$). **Conclusion:** $^{18}$F-ASIS can be safely administered to cancer patients for PET imaging of TF expression in tumors. The trial marks the first test of a TF-targeted PET radiotracer in humans (first-in-class). The findings represent important first steps toward clinical implementation of $^{18}$F-ASIS PET imaging of TF expression.

Received Mar. 4, 2022; revision accepted May 10, 2022.
For correspondence or reprints, contact Andreas Kjaer (akjaer@sund.ku.dk).
*Contributed equally to this work.
Published online May 19, 2022.


**Key Words:** active site inhibited factor VII (ASIS); tissue factor; PET/CT; first-in-humans; phase I clinical trial

**J Nucl Med 2022; 63:1871–1879**
DOI: 10.2967/jnumed.122.264068

Personalized medicine based on targeted therapies is predicted to shape the future of oncology in the coming decades. An emerging oncologic target is the transmembrane glycoprotein tissue factor (TF) that functions as the main initiator of the extrinsic coagulation cascade (*1*). In addition to its role in coagulation, TF expression is also linked to several cancer hallmarks including tumor growth, angiogenesis, and metastatic potential (*2,3*). Abundant TF expression has been reported in most solid tumors, and TF expression levels are associated with disease stage and overall survival in pancreatic cancer (*4*), cervical cancer (*5*), non–small cell lung cancer (*6–8*), and breast cancer (*9*).

TF-targeted therapies are currently under translation into the clinical treatment of cancer patients. In 2019, reports from the first phase 1–2 clinical trial of the TF-targeted antibody–drug conjugate tisotumab vedotin in patients with recurrent, advanced, or metastatic solid tumors showed an objective tumor response in 16% of the patients (*10*). Recently, a 24% response rate was demonstrated in a phase 2 trial in previously treated recurrent or metastatic cervical cancer patients (*11*), and the U.S. Food and Drug Administration approved the therapy in September 2021 for this indication (*12*).

With the emergence of TF-targeted therapies, robust methods for quantifying TF expression in primary tumors and metastases are needed for efficient patient selection and stratification. Whole-body PET imaging can reduce the risk of sampling error from within tumor and between tumor heterogeneity seen in ex vivo analyses of tumor biopsies (*13*). Hence, PET imaging of TF expression is attractive as a companion imaging diagnostic agent for identifying patients eligible for TF-targeted therapies and may have the potential to increase response rates.

We have developed a TF-targeted PET radiotracer based on the natural ligand, factor VII (FVII). When vascular injury occurs, FVII is activated to FVIIa by the exposed TF on the endothelial cells and sets off the coagulation cascade (*1*). Through inhibition of the active site in FVIIa, the resulting active-site inhibited FVIIa (ASIS) binds to TF with an affinity approximately 5-fold higher than FVIIa without activating the coagulation system (*14*). For TF-targeted PET imaging, ASIS is radiolabeled with *N*-succinimidyl 4-[$^{18}$F]fluorobenzoate ($^{18}$F-SFB) to form $^{18}$F-ASIS (*15*). Preclinical studies with xenograft tumor–bearing mice have demonstrated high and specific $^{18}$F-ASIS uptake in tumor tissue that reflects the level of TF expression determined ex vivo (*16*). Spurred on by the promising preclinical results, we moved forward with the clinical translation of $^{18}$F-ASIS PET imaging to cancer patients.

Here we report our first-in-humans trial on $^{18}$F-ASIS PET in cancer patients. The primary objectives were to demonstrate the safety, biodistribution, pharmacokinetics, and dosimetry of $^{18}$F-ASIS. As a secondary objective, we investigated radiotracer accumulation in tumors with PET and its correlation with TF expression in ex vivo analyses of matched tumor samples.

## MATERIALS AND METHODS

### Study Design

We performed the study as an open-label, phase 1 clinical trial approved by the Danish Medicines Agency (EudraCT no. 2015–005583-42) and the Ethical Committee of the Capital Region of Denmark (protocol H-18015477). Patients signed a written informed consent form before inclusion. The study was conducted in accordance with the requirements for good clinical practice including independent monitoring by the Good Clinical Practice unit of Copenhagen University Hospital, and the trial was registered at ClinicalTrials.gov (NCT03790423). Eligible patients were 18 y or older; diagnosed with breast, lung, pancreatic, cervical, or ovarian cancer; and capable of understanding the patient information in Danish and giving full informed consent. Exclusion criteria were pregnancy/breastfeeding, weight above 140 kg, or history of allergic reaction attributable to compounds of similar chemical or biologic composition to $^{18}$F-ASIS.

From January to November 2019, after giving informed consent, 10 patients with pancreatic cancer ($n = 4$), breast cancer ($n = 3$), lung cancer ($n = 2$), and cervical cancer ($n = 1$) were included in the study and referred to a $^{18}$F-ASIS PET/CT imaging series. The mean and SD of the administered mass of $^{18}$F-ASIS was 0.67 ± 0.12 mg (range, 0.41–0.84 mg). The mean administered activity was 157 ± 35 MBq (range, 93–198 MBq), yielding a mean specific activity of 245 ± 84 MBq/mg (range, 126–412 MBq/mg) at the time of injection. Sequential whole-body PET/CT imaging was performed 1, 2, and 4 h after injection of $^{18}$F-ASIS. Patients were monitored for changes in vital signs, electrocardiograms, and blood parameters before and after radiotracer administration. Adverse events were registered up to 48 h after administration of $^{18}$F-ASIS and coded according to the Common Terminology Criteria for Adverse Events (version 5.0). Blood sampling and urine collection was performed for pharmacokinetic analyses. The study design is summarized in Figure 1. A detailed study description is provided in the supplemental information (supplemental materials are available at http://jnm.snmjournals.org). When available, tumor biopsies or surgically excised primary tumor tissue and local lymph nodes were collected, and TF expression was analyzed with immunohistochemistry and enzyme-linked immunosorbent assay (ELISA).

### Inhibition of FVIIa

FVIIa (Novo Nordisk A/S) was dissolved in water and 5 equivalents of D-Phe-Phe-Arg-chloromethyl ketone (fFR-cmk; Bachem) were added for inhibition of FVIIa to produce ASIS. After inhibition (1 h, 4°C), excess of inhibitor was removed by dialysis (Slide-a-lyzer, MWCO 10; Thermo Fisher Scientific) in 50 mM *N*-2-hydroxyethylpiperazine-*N*′-2-ethanesulfonic acid (HEPES,150 mM NaCl, 10 mM $CaCl_2$, pH 7.4; Sigma-Aldrich) overnight. The content of fFR-cmk and the concentration of ASIS were analyzed by high-pressure liquid chromatograph (HPLC) using an Aeris C4 column (3.6 μm, 150 × 4.6 mm; Phenomenex) and 1.5 mL/min solvent flow with a gradient method: 0–2 min 17% B, 2–5 min 60% B, 5–6 min 60% B, 6–7 min 17% B, 7–8 min 17% B with solvent phases 0.1% trifluoroacetic acid (TFA) in $H_2O$ (A) and 0.1% TFA in acetonitrile (MeCN) (B). Aliquots (500 μL) were stored at −80°C before labeling.

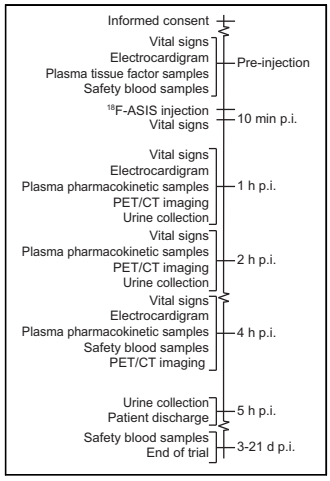


**FIGURE 1.** Schematic overview of study design. p.i. = postinjection.

### Synthesis of $^{18}$F-ASIS

ASIS was labeled with the $^{18}$F-containing prosthetic group $^{18}$F-SFB. $^{18}$F-SFB was produced in a 3-step, 1-pot synthesis on a qualified TracerLab$_{MX}$ module (GE Healthcare) with a final solid-phase extraction purification in 80% MeCN. $^{18}$F-SFB was subsequently evaporated to dryness in a single vial. ASIS (500 μL) was added to the vial for labeling at room temperature for 30 min followed by purification with a PD10 column (Sigma-Aldrich) into formulation buffer (10 mM GlyGly, 150 mM NaCl, and 10 mM $CaCl_2$, pH 7.5). The final product was sterile-filtered in a laminar airflow bench, and a sample was drawn for quality control. The shelf-life of $^{18}$F-ASIS was evaluated up to 4 h after the end of synthesis.

### Quality Control of $^{18}$F-ASIS

All analytic methods were validated according to the International Council of Harmonization guidelines (*17*). The radiochemical purity, unspecified $^{18}$F-labeled impurities, and $^{18}$F-fluoride were determined with radio-HPLC, and the content of ASIS was determined by ultraviolet-detector HPLC, both using the same gradients as described in the "Inhibition of FVIIa" section. Residual MeCN from the $^{18}$F-SFB synthesis was determined by gas chromatography. Color spot tests were used to determine the content of tetrabutylammonium hydrogen carbonate and HEPES in the final product. The immunoreactivity of $^{18}$F-ASIS was determined by Lindmo assay using a high TF-expressing cell line (BxPC-3, CRL-1687; American Type Culture Collection) according to previously described procedures (*18*). Quality control parameters are summarized in Supplemental Table 1.

### Plasma and Urine Pharmacokinetics

The activity of urine, whole blood, and plasma samples was measured on a Cobra II TM γ-Counter (Packard). The plasma samples were prepared from whole-blood samples by centrifugation (3,500 rpm, 4 min) and filtering of the supernatant plasma through a 0.45-μM syringe filter. The radiotracer plasma half-life was determined from the activity concentrations in plasma decay-corrected to the blood sampling time points (approximately 1, 2, and 4 h after injection). The accumulated percentages of excreted radiotracer in urine were determined from the ratio between the accumulated activity in urine and the injected radiotracer activity dose decay-corrected to the urine sampling time points (approximately 1, 2, and 5 h after injection). Metabolites in plasma and urine samples were analyzed by radio-HPLC with a Posi-RAM Module (LabLogic) 4 using the same gradients as described in the "Inhibition of FVIIa" section.

**TABLE 1**
Patient Characteristics

| Characteristic | Patient 1 | 2 | 3 | 4 | 5 | 6 | 7 | 8 | 9 | 10 |
|---|---|---|---|---|---|---|---|---|---|---|
| Sex | Female | Female | Female | Female | Male | Female | Female | Female | Female | Female |
| Age (y) | 88 | 67 | 69 | 79 | 65 | 58 | 54 | 59 | 43 | 73 |
| Primary tumor | Pancreas | Pancreas | Pancreas | Pancreas | Lung† | Lung | Breast | Breast | Cervix | Breast |
| Type [stage]* | PT: DAC | PT: PAC [pT2pN2M0] | PT†: DAC | PT: DAC [pT2N0M0] | PT†: AC MET: AC | PT: AC [pT2bN0M0] | PT: IDC (HER2+1/ ER100%). SN without MET (0/1 LN). [M0] | PT: ILC (HER2+1/ ER100%). SN without MET (0/2 LN). [M0] | PT: SCC | PT‡: ISPC SN with micro MET (1/2 LN). [M0] |
| Prior cancer treatment | None | None | CTX | None | Surgery and CTX | CTX | None | None | None | None |
| Concomitant cancer treatment | None | None | None | None | CTX | RDX | None | None | None | None |

*Pathology TNM staging is reported in square brackets when available.
†Primary tumor removed.
‡Two separate tumors without connection: Tumor 1: HER2+1/ER100%; Tumor 2: HER2-/ER100%.
AC = adenocarcinoma; CTX = chemotherapy; DAC = ductal adenocarcinoma; ER = estrogen receptor; HER2 = human epidermal growth factor receptor 2; IDC = invasive ductal carcinoma; ILC = invasive lobular carcinoma; ISPC = invasive solid papillary carcinoma; LN = lymph nodes; MET = metastases; PAC = pancreaticobiliary adenocarcinoma; PT = primary tumor; RDX = radiation therapy; SCC = squamous cell carcinoma; SN = sentinel nodes.

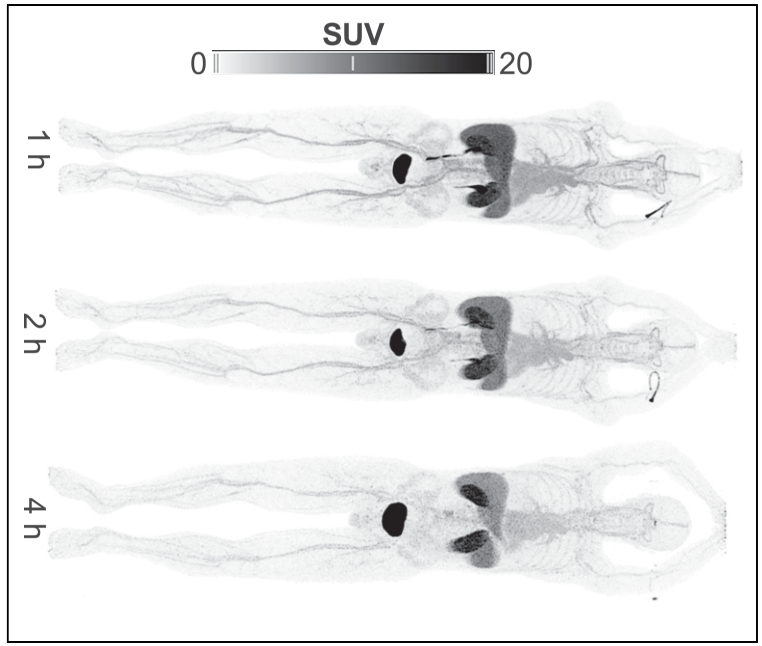


**FIGURE 2.** Representative maximum-intensity projection showing distribution of $^{18}$F-ASIS for patient 5.

### Image Acquisition

Images were acquired on a Biograph 128 mCT PET/CT (Siemens Healthineers) with PET acquisition commenced 1, 2, and 4 h after injection of $^{18}$F-ASIS. Unless otherwise contraindicated, patients were injected with intravenous iodine-based contrast (Optiray [Guerbet] 300 mg I/mL, 70–100 mL, injection rate 1.5–2.5 mL/s) using an automated Medrad Stellant injection system (Bayer). Detailed descriptions of the PET and CT imaging parameters (including acquisition times and reconstruction parameters) are provided in the supplemental materials.

### Biodistribution and Dosimetry

Dosimetry was based on the PET images ($n$ = 10) supplemented with sampled urine data ($n$ = 8). For each patient, organ, and time point, tissue activity concentration was calculated as the average of the mean values from 3 volumes of interests drawn in the following organs/regions: adrenal, bone, brain, blood pool, ascending and descending colon, heart wall, kidney, liver, lung, red marrow (L3–L5 vertebrae), small intestines, spleen, stomach contents, and thyroid using MIRADA DBx, version 1.2.0 (Mirada Medical). OLINDA/EXM 2.0 software (Vanderbilt University and HERMES Medical Solutions) was used for calculation of dosimetry parameters using the organ masses of the OLINDA male adult phantom (*19*,*20*) and the absorbed doses for organs and effective dose with tissue-weighting factors according to International Commission on Radiological Protection (ICRP) 103 (*21*). A detailed description of the dosimetry calculation and biodistribution data processing is provided in the supplemental materials.

### Image Analysis

The PET/CT images were evaluated by a highly experienced team consisting of a nuclear medicine specialist and a radiologist. Size measurements of the primary tumor and metastases (if any) were performed on the diagnostic CT. In tumor lesions identified on the CT, radiotracer accumulation was measured on the PET images and reported as SUVs.

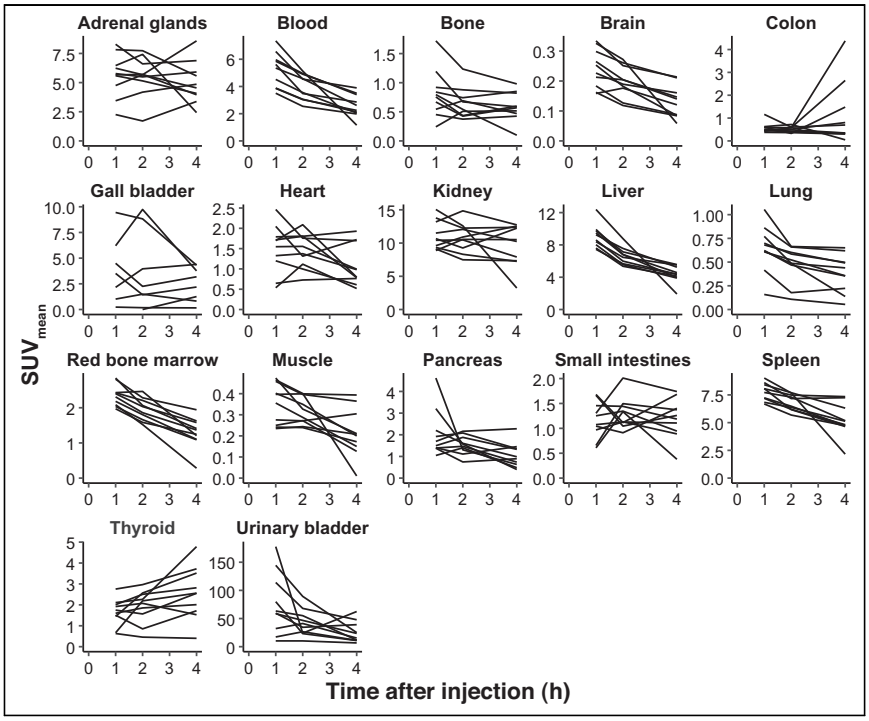


**FIGURE 3.** Distribution of $^{18}$F-ASIS in organs ($n$ = 10).

Spheric volumes of interest maximizing a volume encompassed by the tumor lesion perimeter based on the CT images were used for uptake quantification, and the tumor lesion $SUV_{max}$ and $SUV_{mean}$ were recorded on the PET images. Tumor-to-blood ratios were calculated as tumor lesion $SUV_{max}$ divided by the blood pool $SUV_{mean}$. Any additional foci identified only on PET, judged indicative of a primary tumor or metastases by the readers, were recorded. SyngoVIA (version VB30A-HF04; Siemens Healthineers) was used for the image analysis.

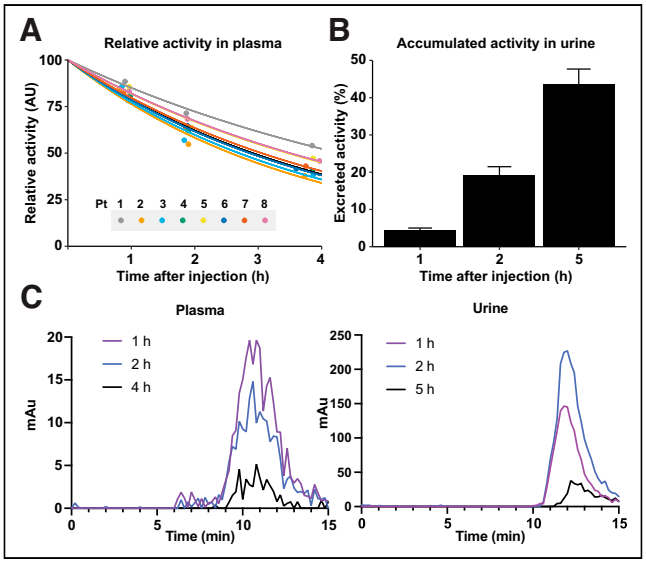


**FIGURE 4.** (A) Normalized time–activity curves of plasma samples with monoexponential fits ($n$ = 8). (B) Accumulated percentages of activity excreted in urine ($n$ = 8). (C) Representative radio-HPLC from plasma showing no major metabolites (left) and representative radio-HPLC from urine showing urinary excretion of a smaller $^{18}$F-radiolabeled fragment (right). AU = arbitrary units; mAu = absorbance units.

### Ex Vivo Tumor Tissue Samples

Tumor tissue samples were obtained from surgically resected tissue or from tumor biopsies performed in relation to routine clinical procedures. Samples were processed for measurement of TF expression with ELISA and immunohistochemistry. Details on tissue preparation, ELISA measurements, and immunohistochemistry preparation are provided in the supplemental materials. TF expression on immunohistochemistry was stratified as low, intermediate, or high based on visual assessment.

### Statistical Methods

The radiotracer plasma half-life was determined from monoexponential linear regression models (1-compartment models) fitted to the decay-corrected time–activity curves in plasma ($n$ = 8). The relationship between the 4-h PET tumor $SUV_{max}$ and ex vivo measurements of TF expression by ELISA was analyzed with Pearson correlation ($n$ = 5). Two-sided $P$ values of less than 0.05 were considered statistically significant. Data are presented as mean ± SD unless otherwise noted. All statistical analyses were performed using R, version 3.6.1 (R Foundation for Statistical Computing).

## RESULTS

### Radiochemistry

$^{18}$F-SFB was prepared in 29.4% ± 25.9% non–decay-corrected radiochemical yield ($n$ = 10 batches). $^{18}$F-ASIS was achieved in 221 ± 58 MBq non–decay-corrected activity yield ($n$ = 10 batches). $^{18}$F-ASIS was produced with a radiochemical purity ≥ 95%, and unspecified $^{18}$F-labeled impurities and $^{18}$F-fluoride were both determined to be ≤2%. The concentration of ASIS was 0.08 ± 0.01 mg/mL. Tetrabutylammonium hydrogen carbonate and HEPES content were <0.1 mg/mL and <20 μg/mL, respectively. An immunoreactivity of ≥75% was found for all 10 batches. Summary results of all quality control parameters are provided in Supplemental Table 1.

### Patient Characteristics and Safety

The characteristics of the patients are shown in Table 1. There were no adverse events and no clinically significant changes in vital signs (Supplemental Table 2), blood parameters (Supplemental Table 3), or electrocardiograms observed in any of the 10 patients.

### Biodistribution, Pharmacokinetics, and Dosimetry

*Biodistribution.* A representative imaging series demonstrating the radiotracer distribution on the 1-, 2-, and 4-h PET on the maximum-intensity projection is shown in Figure 2 for patient 5. The maximum-intensity projections for the additional 9 patients are shown in Supplemental Figure 1. Organ-specific radiotracer uptake expressed as $SUV_{mean}$ is shown in Figure 3. The highest uptake was observed in the urinary bladder followed by the kidneys and the liver. The brain, bone, muscle, red bone marrow, and lung had low and decreasing uptake, suggesting no radiotracer accumulation.

*Pharmacokinetics and Dosimetry.* Time–activity curves measured in plasma ($n$ = 8) are shown in Figure 4A. The plasma half-life was 3.2 ± 0.6 h. Urinary excretion accounted for most of the $^{18}$F-ASIS elimination, and more than 40% of the injected

**TABLE 2**
Organ-Based Dosimetry

| Organ | Total mean absorbed dose (μGy/MBq) |
|---|---|
| Adrenals | 56 |
| Brain | 4 |
| Breasts | 8 |
| Esophagus | 12 |
| Eyes | 6 |
| Gallbladder wall | 22 |
| Left colon | 21 |
| Small intestine | 25 |
| Stomach wall | 15 |
| Right colon | 13 |
| Rectum | 17 |
| Heart wall | 17 |
| Kidneys | 76 |
| Liver | 67 |
| Lungs | 10 |
| Ovaries | 15 |
| Pancreas | 17 |
| Prostate | 15 |
| Salivary glands | 7 |
| Red marrow | 15 |
| Osteogenic cells | 16 |
| Spleen | 60 |
| Testes | 8 |
| Thymus | 9 |
| Thyroid | 17 |
| Urinary bladder wall | 118 |
| Uterus | 22 |
| Total body | 12 |
| Effective dose (μSv/MBq) | 20 |

activity was accumulated in the urine within 5 h after injection (Fig. 4B). Radio-HPLC run on plasma samples showed no major metabolites. Radio-HPLC run on urine samples showed urinary excretion of a smaller $^{18}$F-radiolabeled fragment, suggesting renal metabolism of $^{18}$F-ASIS. Representative chromatograms of plasma samples collected 1, 2, and 4 h after injection and urine samples collected 1, 2, and 5 h after injection are shown in Figure 4C. The dosimetry output from the OLINDA/EXM dosimetry software is shown in Table 2. The highest dose was received by the urinary bladder wall (118 μGy/MBq) followed by the kidneys (76 μGy/MBq), liver (67 μGy/MBq), and spleen (60 μGy/MBq). The effective dose was 20 μSv/MBq corresponding to 4 mSv for a target activity of 200 MBq.

### Radiotracer Accumulation in Tumor and Correlation with Ex Vivo Tumor Tissue

$^{18}$F-ASIS accumulation in tumor lesions quantified as $SUV_{max}$ and tumor-to-blood ratios are shown in Figure 5. Heterogeneous $SUV_{max}$ patterns between patients were observed: for patients 3 and 4 (both primary pancreatic tumors) and 5 (lung metastasis) $SUV_{max}$ increased on the 2- to 4-h PET compared with the 1-h PET. Contrary, in patients 7 and 8 (both primary breast tumors), low uptake was observed at all 3 time points. The remaining patients showed relatively intermediate $SUV_{max}$ that remained stable or slightly increased with time. Compared with the other patients, for patients 3 and 4 the 4-h PET $SUV_{max}$ was relatively high. The tumor-to-blood ratios showed a similar pattern.

Within tumor and within patient heterogeneity in radiotracer accumulation was also observed. Patient 10 (breast cancer) had heterogeneous radiotracer accumulation in the primary tumor (Fig. 6A), with 4-h PET $SUV_{max}$ in the intermediate range (2.86).

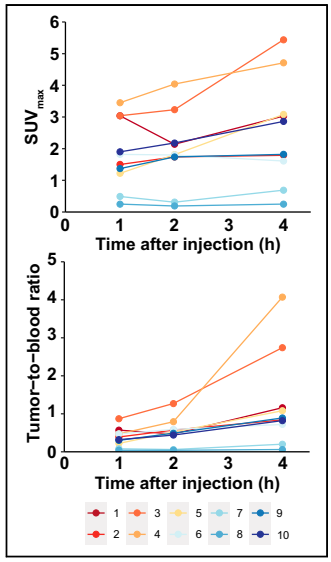


**FIGURE 5.** Tumor $SUV_{max}$ (top) and tumor-to-blood ratios (tumor $SUV_{max}$ divided by blood pool $SUV_{mean}$) on 1-, 2-, and 4-h PET (bottom). Colors refer to patient numbers.

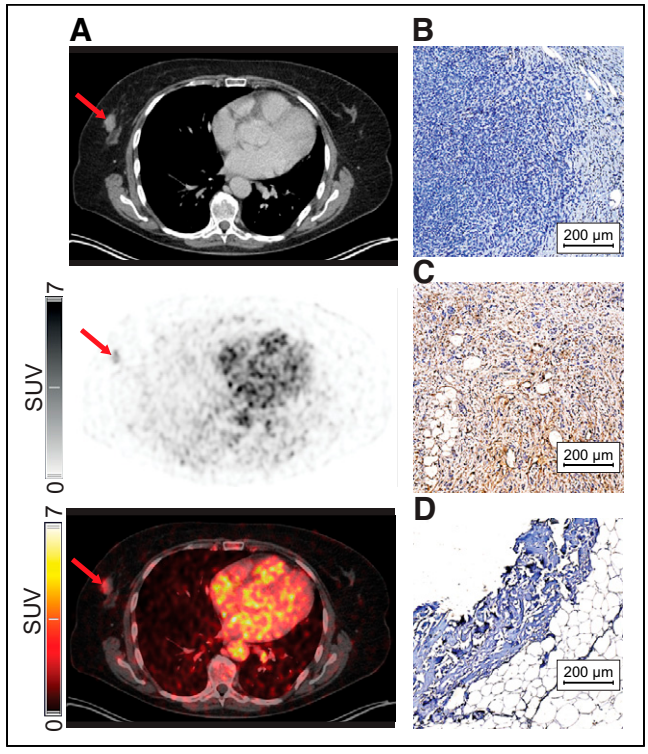


**FIGURE 6.** Patient 10 with breast cancer. (A) Primary breast tumor with relatively intermediate 4-h PET $SUV_{max}$ (2.86) shown on (from top to bottom) CT, PET, and fused PET/CT. Arrows mark tumor location. (B) Small sample taken from tumor lesion immediately after surgery with low TF expression on immunohistochemistry. (C) Portion of mastectomy specimen showing intermediate TF expression in the tumor on immunohistochemistry performed after pathology examination. (D) Axillary sentinel node metastasis with low TF expression on immunohistochemistry without apparent focal accumulation in corresponding axillary area on PET or lymph node enlargement on CT (not shown).

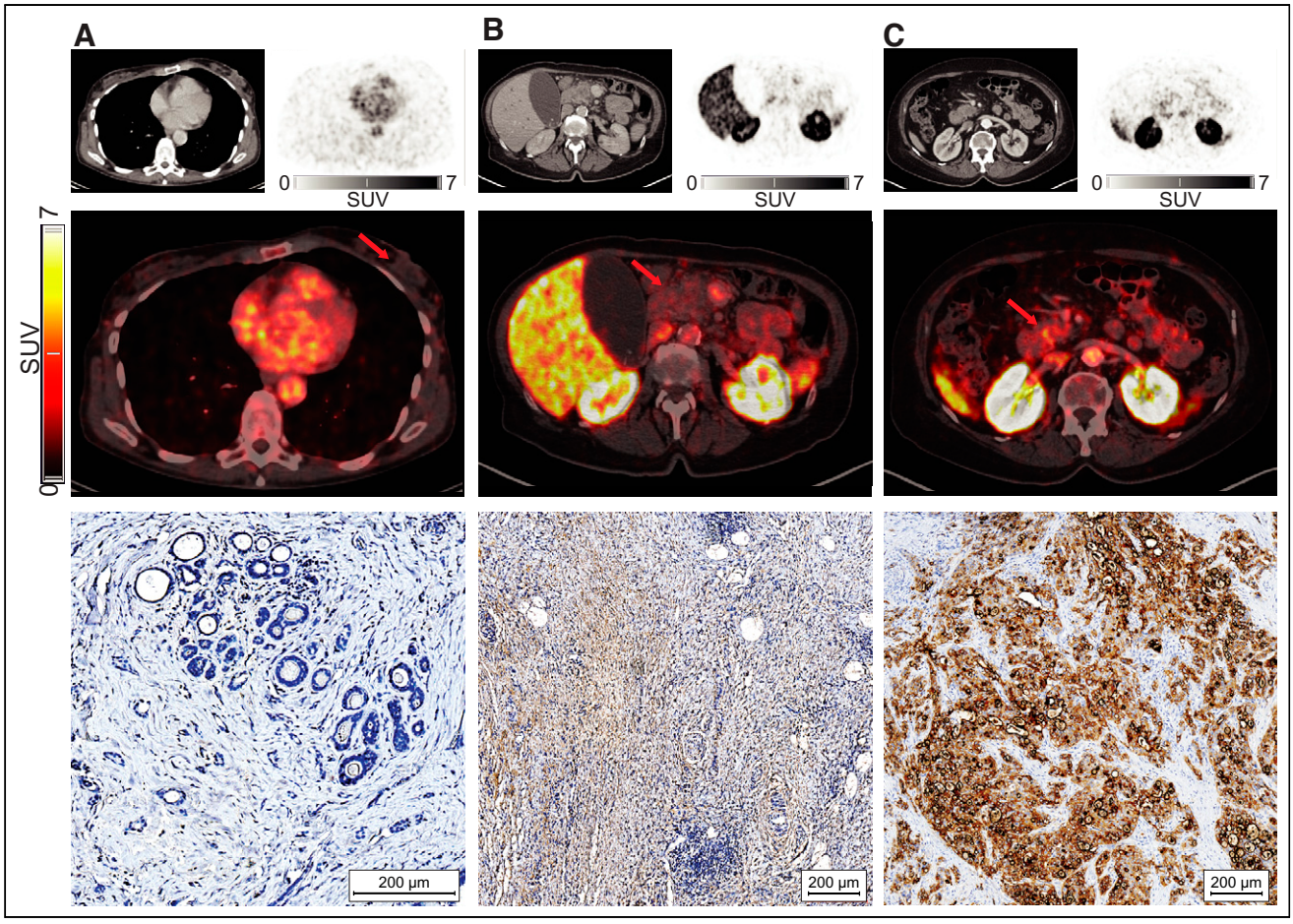


**FIGURE 7.** (A) Patient 7: breast tumor with low 4-h PET $SUV_{max}$ (0.69) and low TF expression on immunohistochemistry ex vivo. (B) Patient 2: pancreatic tumor with relatively intermediate 4-h PET $SUV_{max}$ (1.79) and intermediate TF expression on immunohistochemistry. (C) Patient 4: pancreatic tumor with relatively high 4-h PET $SUV_{max}$ (4.71) and high TF expression on immunohistochemistry. Images from top to bottom are: 4-h CT, PET and fused PET/CT, and immunohistochemistry. Arrows mark tumor location on PET/CT.

A corresponding small tissue sample taken immediately from the surgically resected tumor showed low ex vivo TF expression measured with both ELISA and immunohistochemistry (Fig. 6B). However, TF immunohistochemistry staining of the tumor from the full mastectomy specimen, performed after the pathology examination, showed areas with intermediate TF expression (Fig. 6C). The pathology examination demonstrated 2 separate primary tumors. This patient also had an axially sentinel node metastasis that was not enlarged on CT, showed no apparent focal accumulation on PET, and had low TF expression on immunohistochemistry (Fig. 6D).

There was a trend of a positive correlation between 4-h PET $SUV_{max}$ and TF expression measured ex vivo on matched tumor tissue samples, although not statistically significant ($r = 0.84$, $P = 0.08$, $n = 5$). TF immunohistochemistry stains in matched tumor tissue samples were available for 7 patients. Representative examples of low, intermediate, and high TF expression on immunohistochemistry with corresponding 4-h PET/CT images are shown in Figure 7. A summary of the PET/CT findings, quantitative plasma and ex vivo tumor TF expression, and TF immunohistochemistry staining patterns is shown in Table 3.

## DISCUSSION

We report here the first-in-humans experience of the TF-targeted radiotracer $^{18}$F-ASIS in cancer patients. The trial marks the first test in humans of a PET radiotracer targeting TF (first-in-class). Our main finding was that injection of $^{18}$F-ASIS was safe, and no adverse events were observed. The effective radiation dose of 4 mSv from administration of 200 MBq of $^{18}$F-ASIS is lower than that received after a standard $^{18}$F-FDG injection (*22*). None of the calculated organ-specific absorbed doses were prohibitive for administration of 200 MBq of $^{18}$F-ASIS. As an indication of the specific tumor-targeting ability of $^{18}$F-ASIS, we observed a trend of a positive correlation between tumor $SUV_{max}$ and quantitative TF expression determined ex vivo ($r = 0.84$, $P = 0.08$). These initial findings represent important first steps toward the clinical implementation of $^{18}$F-ASIS PET imaging as a companion diagnostic tool for TF-targeted therapies.

The biodistribution and pharmacokinetic data indicated that the primary elimination route of $^{18}$F-ASIS was through the kidneys. The low bone uptake is supportive of high metabolic stability, as freely circulating $^{18}$F-fluoride would expectedly result in high bone accumulation (*23*). The 3.2-h $^{18}$F-ASIS plasma half-life was comparable to the 3.8-h plasma half-life observed for an unlabeled version of ASIS at similar dose (*24*), suggesting that the radiolabeling does not fundamentally alter the elimination of the radiotracer from plasma. Compared with antibody- and antibody fragment–based TF-targeted radiotracers with long circulation time resulting in optimal tumor-to-background contrast after several days in preclinical

**TABLE 3**
PET/CT Image Findings and Ex Vivo Tissue Factor Measurements

| Characteristic | Patient | | | | | | | | | |
|---|---|---|---|---|---|---|---|---|---|---|
| | 1 | 2 | 3 | 4 | 5 | 6 | 7 | 8 | 9 | 10 |
| Primary tumor | Pancreas | Pancreas | Pancreas | Pancreas | Lung‖ | Lung | Breast | Breast | Cervix | Breast |
| Radiotracer mass (mg) | 0.84 | 0.69 | 0.71 | 0.71 | 0.74 | 0.41 | 0.76 | 0.56 | 0.74 | 0.58 |
| Injected activity (MBq) | 135 | 187 | 198 | 189 | 93 | 169 | 145 | 187 | 117 | 145 |
| Specific activity* (MBq/mg) | 161 | 271 | 279 | 266 | 126 | 412 | 191 | 334 | 158 | 250 |
| Metastases (Pathology/PET/CT)† | ÷/÷/÷ | ÷/÷/÷ | ÷/÷/÷ | ÷/÷/÷ | +/+/+ | ÷/÷/÷ | ÷/÷/÷ | ÷/÷/÷ | ÷/÷/÷ | +/÷/÷¶ |
| Tumor size (cm) | 3.6 × 3.3 | 3.5 × 3.1 | 4.9 × 3.8 | 2.6 × 2.2 | 1.2 × 0.9‖ | 3.6 × 3.4 | 2.8 × 1.4 | 0.7 × 0.8 | 3.2 × 2.9 | 2.4 × 1.4 |
| Tumor $SUV_{max}$ | | | | | | | | | | |
| 1 h | 3.04 | 1.50 | 3.04 | 3.45 | 1.22‖ | 1.82 | 0.49 | 0.25 | 1.37 | 1.90# |
| 2 h | 2.14 | 1.74 | 3.23 | 4.04 | 1.81‖ | 1.80 | 0.31 | 0.19 | 1.74 | 2.18# |
| 4 h | 3.03 | 1.79 | 5.44 | 4.71 | 3.08‖ | 1.61 | 0.69 | 0.25 | 1.82 | 2.86# |
| Tumor $SUV_{mean}$ | | | | | | | | | | |
| 1 h | 1.41 | 0.85 | 1.67 | 1.93 | 0.83‖ | 0.70 | 0.30 | 0.20 | 0.75 | 1.19# |
| 2 h | 1.38 | 0.96 | 1.73 | 2.24 | 1.19‖ | 1.26 | 0.21 | 0.15 | 0.92 | 1.21# |
| 4 h | 1.68 | 0.98 | 2.94 | 2.62 | 1.97‖ | 1.18 | 0.40 | 0.15 | 1.01 | 1.73# |
| ΔT (d)‡ | 42 | 4 | NA | 6 | NA | NA | 12 | 5 | 6 | 4 |
| $TF_{tumor}$ (μg/mg) | NA | 5.93 | NA | 25.75 | NA | NA | 1.14 | NA | 1.27** | PT: 0.67<br>MET: NA |
| $TF_{tumor}$ IHC§ | Low** | Intermediate | NA | High | NA | NA | Low | Low | Low** | PT: Low/intermediate††<br>MET: Low |
| $TF_{plasma}$ (μg/L) | 61 | 54 | 56 | 72 | 73 | 43 | 82 | 66 | 21 | 73 |

*At time of injection.
†Presence of metastases based on pathology, PET, and CT, respectively.
‡Time between imaging and tissue collection.
§TF expression on immunohistochemistry (IHC) rated low, intermediate, or high based on visual assessment.
‖Primary tumor removed. SUV and size measured on metastasis.
¶No lymph node enlargement on CT and no apparent focal accumulation on PET.
#Heterogeneous radiotracer accumulation observed.
**Samples from biopsies.
††Low TF staining on IHC on tissue sample also showing low (0.67 μg/mg) TF expression. Tissue from full mastectomy, obtained from postpathology evaluation, with intermediate TF expression on IHC.
+ = metastases present; ÷ = no metastases; MET = metastases; NA = not available; PT = primary tumor.

models, for example, $^{64}$Cu- and $^{89}$Zr-labeled ALT-836 (*25,26*), the relatively fast elimination of $^{18}$F-ASIS makes this radiotracer better suited for same-day imaging.

The between-patient and cancer type heterogeneity in radiotracer tumor accumulation and ex vivo tumor TF expression observed in the study is in line with the varying degree of TF expression across cancer types reported in the literature (*2,16,27*). Pancreatic tumors have particularly high TF expression in agreement with our findings. The within-tumor heterogeneity seen in both radiotracer accumulation on PET and on ex vivo TF immunohistochemistry staining of the tumor from the full surgical specimens serves as an example of the potential of PET imaging for evaluation of TF expression. As PET imaging captures the whole-body tumor burden, identification of hotspots that could be otherwise missed on a biopsy is possible with PET. Importantly, the sentinel node metastasis without enlargement on CT, and with no apparent focal PET accumulation, had low TF expression on immunohistochemistry, which suggests that PET was not false-negative. Conclusions should not, of course, be inferred from single observations, but the results encourage further investigation.

The trend of a positive correlation between tumor $SUV_{max}$ and quantitative TF expression measured ex vivo ($r = 0.84$, $P = 0.08$) suggests that $^{18}$F-ASIS accumulation depends on the levels of TF in tumors. It may be argued that the radiotracer accumulation in tumors was modest. Importantly, this does not pose a limitation to the use of $^{18}$F-ASIS PET as a whole-body noninvasive companion diagnostic or prognostic tool based on tumor TF expression if robust correlations between PET-derived tumor radiotracer accumulation and actual TF expression can be established. The relationship between $SUV_{max}$ and ex vivo TF expression presented in this study suggests such a correlation. The observed trend is in line with our preclinical results in xenografted tumor mouse models that showed a strong and statistically significant positive correlation between tumor $SUV_{max}$ on 4-h $^{18}$F-ASIS PET and TF expression measured in excised tumor tissue (*16*). The specificity of $^{18}$F-ASIS for targeting TF was supported by the qualitative relationship between the tumor $SUV_{max}$ and TF immunohistochemistry staining patterns of surgical specimens that generally were in agreement. These preliminary results suggest that $^{18}$F-ASIS PET imaging can be used for noninvasive measurement of TF expression in tumor tissues, which may ultimately assist in identifying patients eligible for TF-targeted therapies. However, future later-phase clinical studies are needed to validate these findings in larger populations.

## CONCLUSION

$^{18}$F-ASIS can safely be administered to cancer patients for TF-targeted PET imaging. The trial marks the first test of a TF-targeted PET radiotracer in humans (first-in-class). The effective whole-body dose from injection of 200 MBq was 4 mSv and no prohibitive organ-specific absorbed doses were observed. Plasma half-life was 3.2 h, and renal elimination accounted for most of the radiotracer excretion. The findings represent important first steps toward the clinical implementation of $^{18}$F-ASIS for PET imaging of TF expression, which could assist in patient prognostication and selection of eligible patients for TF-targeted therapies. Future later-phase studies are needed to validate these initial findings.

## DISCLOSURE

This project received funding from the European Union's Horizon 2020 research and innovation program under grant agreements no. 670261 (ERC Advanced Grant) and 668532 (Click-It), the Lundbeck Foundation, the Novo Nordisk Foundation, the Innovation Fund Denmark, the Danish Cancer Society, Arvid Nilsson Foundation, the Neye Foundation, the Research Foundation of Rigshospitalet, the Danish National Research Foundation (grant 126), the Research Council of the Capital Region of Denmark, the Danish Health Authority, the John and Birthe Meyer Foundation and Research Council for Independent Research. Andreas Kjaer and Carsten H. Nielsen are inventors/hold intellectual property rights on a patent covering tissue factor imaging. Andreas Kjaer is a Lundbeck Foundation Professor. No other potential conflict of interest relevant to this article was reported.

## ACKNOWLEDGMENTS

We are grateful to the staff at the Department of Clinical Physiology and Nuclear Medicine for help with performing the PET/CT studies and for the patients for participating in the study. We also thank Katrine Qvist for performing the ex vivo immunohistochemistry staining and ELISA measurements. Novo Nordisk A/S is gratefully acknowledged for providing GMP-grade FVIIa.

## KEY POINTS

**QUESTION:** Can $^{18}$F-ASIS safely be administered to cancer patients for PET imaging of TF in tumors?

**PERTINENT FINDINGS:** In this first-in-humans clinical trial of 10 cancer patients, administration of $^{18}$F-ASIS was safe, and no adverse events were reported. The effective whole-body dose was 4 mSv for injection of a target activity of 200 MBq, and no prohibitive organ-specific absorbed doses were observed.

**IMPLICATIONS FOR PATIENT CARE:** The trial marks the first test in humans of a PET radiotracer targeting TF (first-in-class). The findings represent important first steps toward implementation of $^{18}$F-ASIS PET imaging of TF in cancer patients for prognostication and selection of patients for TF-targeted therapies.

## REFERENCES

1. McVey JH. Tissue factor pathway. *Baillieres Clin Haematol.* 1994;7:469–484.
2. van den Berg YW, Osanto S, Reitsma PH, Versteeg HH. The relationship between tissue factor and cancer progression: insights from bench and bedside. *Blood.* 2012;119:924–932.
3. Kasthuri RS, Taubman MB, Mackman N. Role of tissue factor in cancer. *J Clin Oncol.* 2009;27:4834–4838.
4. Nitori N, Ino Y, Nakanishi Y, et al. Prognostic significance of tissue factor in pancreatic ductal adenocarcinoma. *Clin Cancer Res.* 2005;11:2531–2539.
5. Zhao X, Cheng C, Gou J, et al. Expression of tissue factor in human cervical carcinoma tissue. *Exp Ther Med.* 2018;16:4075–4081.
6. Regina S, Valentin JB, Lachot S, Lemarie E, Rollin J, Gruel Y. Increased tissue factor expression is associated with reduced survival in non-small cell lung cancer and with mutations of TP53 and PTEN. *Clin Chem.* 2009;55:1834–1842.
7. Goldin-Lang P, Tran QV, Fichtner I, et al. Tissue factor expression pattern in human non-small cell lung cancer tissues indicate increased blood thrombogenicity and tumor metastasis. *Oncol Rep.* 2008;20:123–128.
8. Chen WH, Wang C, Zhang YH, Yang YH, Zhan HY, Zhang LM. Influence of overexpressed coagulant and fibrolytic components in tumor tissues on the prognosis of non-small cell lung cancer. *Zhonghua Yi Xue Za Zhi.* 2007;87:3228–3232.
9. Ueno T, Toi M, Koike M, Nakamura S, Tominaga T. Tissue factor expression in breast cancer tissues: Its correlation with prognosis and plasma concentration. *Br J Cancer.* 2000;83:164–170.
10. de Bono JS, Concin N, Hong DS, et al. Tisotumab vedotin in patients with advanced or metastatic solid tumours (InnovaTV 201): a first-in-human, multicentre, phase 1-2 trial. *Lancet Oncol.* 2019;20:383–393.

11. Coleman RL, Lorusso D, Gennigens C, et al. Efficacy and safety of tisotumab vedotin in previously treated recurrent or metastatic cervical cancer (InnovaTV 204/GOG-3023/ENGOT-cx6): A multicentre, open-label, single-arm, phase 2 study. *Lancet Oncol.* 2021;22:609–619.
12. U.S. Food and Drug Administration (FDA). Orange book: approved drug products with therapeutic equivalence evaluations. U.S. FDA website. https://www.accessdata.fda.gov/drugsatfda_docs/label/2021/761208s000lbl.pdf. Accessed September 30, 2022.
13. Subramaniam RM. Precision medicine and PET/computed tomography: challenges and implementation. *PET Clin.* 2017;12:1–5.
14. Sorensen BB, Persson E, Freskgard PO, et al. Incorporation of an active site inhibitor in factor VIIa alters the affinity for tissue factor. *J Biol Chem.* 1997;272:11863–11868.
15. Erlandsson M, Nielsen CH, Jeppesen TE, et al. Synthesis and characterization of $^{18}$F-labeled active site inhibited factor VII (ASIS). *J Labelled Comp Radiopharm.* 2015;58:196–201.
16. Nielsen CH, Erlandsson M, Jeppesen TE, et al. Quantitative PET imaging of tissue factor expression using $^{18}$F-labeled active site-inhibited factor VII. *J Nucl Med.* 2016;57:89–95.
17. European Medicines Agency (EMA). ICH harmonised tripartite guideline: validation of analytical methods[em dash]methodology. In: *ICH Topic Q2(R1) Validation of Analytical Procedures: Text and Methodology*. CPMP/ICH/381/95. London: EMEA; 2006:7–15.
18. Lindmo T, Boven E, Cuttitta F, Fedorko J, Bunn PA Jr. Determination of the immunoreactive fraction of radiolabeled monoclonal antibodies by linear extrapolation to binding at infinite antigen excess. *J Immunol Methods.* 1984;72:77–89.
19. International Commission on Radiological Protection (ICRP). Basic anatomical and physiological data for use in radiological protection: reference values—a report of age- and gender-related differences in the anatomical and physiological characteristics of reference individuals. ICRP publication 89. *Ann ICRP.* 2002;32:5–265.
20. Stabin MG, Siegel JA. Physical models and dose factors for use in internal dose assessment. *Health Phys.* 2003;85:294–310.
21. International Commission on Radiological Protection (ICRP). The 2007 recommendations of the International Commission on Radiological Protection. ICRP publication 103. *Ann ICRP.* 2007;37:1–332.
22. Quinn B, Dauer Z, Pandit-Taskar N, Schoder H, Dauer LT. Radiation dosimetry of $^{18}$F-FDG PET/CT: incorporating exam-specific parameters in dose estimates. *BMC Med Imaging.* 2016;16:41.
23. Ahuja K, Sotoudeh H, Galgano SJ, et al. $^{18}$F-sodium fluoride PET: history, technical feasibility, mechanism of action, normal biodistribution, and diagnostic performance in bone metastasis detection compared with other imaging modalities. *J Nucl Med Technol.* 2020;48:9–16.
24. Erhardtsen E, Nilsson P, Johannessen M, Thomsen MS. Pharmacokinetics and safety of FFR-rFVIIa after single doses in healthy subjects. *J Clin Pharmacol.* 2001;41:880–885.
25. Hong H, Zhang Y, Nayak TR, et al. Immuno-PET of tissue factor in pancreatic cancer. *J Nucl Med.* 2012;53:1748–1754.
26. Hernandez R, England CG, Yang Y, et al. ImmunoPET imaging of tissue factor expression in pancreatic cancer with $^{89}$Zr-Df-ALT-836. *J Control Release.* 2017;264:160–168.
27. Saidak Z, Soudet S, Lottin M, et al. A pan-cancer analysis of the human tumor coagulome and its link to the tumor immune microenvironment. *Cancer Immunol Immunother.* 2021;70:923–933.